Extreme and superextreme events in a loss-modulated CO_2 laser: Nonlinear resonance route and precursors

Cristian Bonatto and Antonio Endler
Instituto de Física, Universidade Federal do Rio Grande do Sul, 91501-970 Porto Alegre, Brazil
(Received 7 December 2016; revised manuscript received 8 April 2017; published 18 July 2017)

We investigate the occurrence of extreme and rare events, i.e., giant and rare light pulses, in a periodically modulated CO_2 laser model. Due to nonlinear resonant processes, we show a scenario of interaction between chaotic bands of different orders, which may lead to the formation of extreme and rare events. We identify a crisis line in the modulation parameter space, and we show that, when the modulation amplitude increases, remaining in the vicinity of the crisis, some statistical properties of the laser pulses, such as the average and dispersion of amplitudes, do not change much, whereas the amplitude of extreme events grows enormously, giving rise to extreme events with much larger deviations than usually reported, with a significant probability of occurrence, i.e., with a long-tailed non-Gaussian distribution. We identify recurrent regular patterns, i.e., precursors, that anticipate the emergence of extreme and rare events, and we associate these regular patterns with unstable periodic orbits embedded in a chaotic attractor. We show that the precursors may or may not lead to the emergence of extreme events. Thus, we compute the probability of success or failure (false alarm) in the prediction of the extreme events, once a precursor is identified in the deterministic time series. We show that this probability depends on the accuracy with which the precursor is identified in the laser intensity time series.

DOI: 10.1103/PhysRevE.96.012216

I. INTRODUCTION

Many natural and engineered systems can exhibit extreme and rare events. *Extreme* means that the events have large magnitude when compared with the average magnitude of their statistical distribution, and *rare* means that the extreme events (EEs) have a low probability of occurrence. Despite the fact that EEs have a low probability of occurrence, many systems have shown situations in which the probability of occurrence of the EEs is significantly higher than expected from Gaussian distributions. Recently, investigations on EEs have received a considerable amount of attention from the scientific community, especially in the context of rogue or freak wave phenomena in hydrodynamics and optics [1–6], but also in other contexts including geophysics, space plasmas, and finance [7–9].

The interest in the subject is justified by several factors. One is due to practical reasons, for example the obvious destructive power that such events could result in different contexts. Other factors include the generality of the phenomenon, that is, a wide variety of different systems may exhibit EEs, and the fact that EEs are associated with very complicated dynamics, including chaotic and turbulent regimes. Such situations are less known and exploited than more regular situations usually investigated in different models and systems, which appear in many contexts.

In recent years, many efforts have been made to increase our understanding of the dynamics of EEs. From a theoretical point of view, EEs are often described or investigated in modeling based on partial differential equations (PDEs), ordinary differential equations (ODEs), or delay differential equations (DDEs). In the case of PDEs, EEs involve spatiotemporal dynamics (in many cases they are called *rogue*, *freak*, *extreme*, or *giant waves*). In the case of ODEs or DDEs, EEs involve only temporal dynamics. Among the main problems that have been considered, two themes have received a great deal attention. One is with respect to the *mechanisms* responsible for the appearance of EEs, and the other concerns the *predictability* of EEs.

The origin of EEs has been the subject of intense debate. In fact, different systems or levels of description have revealed various mechanisms responsible for the formation of EEs. The emergence of EEs has been associated with linear and nonlinear regimes. The generation of EEs in linear systems has been reported by different authors [10–16]. With respect to nonlinear systems, the most prominent case, generally accepted as forming the EEs (in the context of rogue waves studies), is the Benjamin-Feir (or modulational) instability [17–21]. This condition has recently been questioned for the case of ocean waves [22]. Other nonlinear scenarios associated with EE formation include chaotic dynamics in low-dimensional systems [23], stochastically induced transitions in multistable systems [24], collisions of breather-solitons [25], integrable turbulence [26], spatiotemporal chaos [27], vortex dynamics [28], vortex turbulence [29], and delayed-feedback systems [30,31]. In the case of low-dimensional chaotic systems, *crises* have been identified as one of the mechanisms associated with the emergency of EEs [32], and they have recently received some attention [33–35].

Another issue of great interest in EE study, of obvious practical importance, is the possibility to predict rare events of great magnitude with some advance in time. As the subject is very interdisciplinary, many efforts, in different contexts, have been directed to this problem (see, e.g., [36–39]). Due to the possibility of EEs being associated with a deterministic origin, some degree of predictability is expected in these situations. Recently, some progress has been made in this direction, with the most sound result being the identification of certain regular patterns that occur anticipating the emergence of EEs [32,35,40].

The aim of this manuscript is to investigate some novel aspects related to these two important points in the study of EEs, that is, the mechanism of formation and the predictability of EEs, using a relatively simple low-dimensional and

deterministic chaotic system, namely a periodically modulated CO_2 laser. Concerning the mechanism, we identify a crisis line in the parameter space of the CO_2 laser model, and we investigate the emergence of EEs in the vicinity and along this line. We show that, when the modulation amplitude is increased (staying in the vicinity of the crisis), the average and dispersion of the laser pulse amplitudes do not increase much, but the amplitude of EEs increases enormously. Usually, EEs are found with amplitudes exceeding slightly four or eight standard deviations over the average amplitude of the events. Here, we show EEs that significantly exceed this criterion. We call these "superextreme events" (SEEs), in analogy to the discovery of "super rogue waves" in a hydrodynamical system [41], and we explain their formation in terms of a nonlinear resonance route. We present a comprehensive study on the formation of extreme and rare events along a two-parameter space, where we show the evolution of EEs with deviations that increase progressively, and, importantly, we show that large-deviation events are related to solutions of different orders. We further perform an original study of the behavior of the coefficient of variation of the chaotic dynamics of laser intensity when crossing a transition between chaotic attractors with very different statistical properties, which helps us to understand the dynamics of extremely large deviation events. With regard to the prediction of EEs, as we mentioned above, recent results show that there are regular patterns that anticipate the occurrence of EEs. However, a more detailed study of these regular patterns has not yet been performed. Here we shed some light on this subject. Specifically, (a) we show that these regular patterns can appear without the emergence of EEs (i.e., we can have false alarms), (b) we associate the oscillation period of these regular patterns with certain unstable periodic orbits embedded in the laser chaotic dynamics, and (c) we investigate the probability of predicting EEs in terms of the precision with which we can find a precursor in the time series.

II. MODEL

The single-mode dynamics of the loss-modulated CO_2 laser involves two coupled degrees of freedom and a time-dependent parameter, which we write, as usual [42–44],

$$\begin{aligned} \frac{dI}{dt} &= \frac{1}{\tau}(N-k)I, \\ \frac{dN}{dt} &= (N_0-N)\gamma - IN. \end{aligned} \tag{1}$$

Here, I is proportional to the laser intensity, N and N_0 are the gain and unsaturated gain in the medium, respectively, τ denotes the transit time of the light in the laser cavity, γ is the gain decay rate, and $k \equiv k(t)$ represents the total cavity losses. The losses are modulated periodically as

$$k(t) = k_0(1 + a\cos 2\pi f t), \tag{2}$$

where k_0 is the constant part of the losses, and a and f are the amplitude and frequency of the modulation, respectively. The parameters a and f are varied in the numerical simulations. The remaining parameters are fixed at $\gamma = 1.978 \times 10^5\ \mathrm{s}^{-1}$, $\tau = 3.5 \times 10^{-9}$ s, $N_0 = 0.175$, and $k_0 = 0.17$. Integrations were done using the standard fourth-order Runge-Kutta scheme with a fixed time step, equal to $h = 2 \times 10^{-8}$.

In the absence of modulation ($k = k_0$), the laser behaves like a damped oscillator. From an initial operating condition, the laser output power displays damped relaxation oscillations converging to a steady state given by

$$I_S = \gamma\left(\frac{N_0}{k_0} - 1\right), \tag{3}$$

$$N_S = k_0, \tag{4}$$

where the relaxation oscillation frequency is given by

$$f_{\mathrm{RO}} \approx \frac{1}{2\pi}\sqrt{\frac{\gamma k_0}{\tau}\left(\frac{N_0}{k_0} - 1\right)}, \tag{5}$$

where we used the fact that the CO_2 laser is a class-B laser [44]. When the modulation parameters (a, f) are turned on, the laser displays a complicated set of resonances and instabilities, which may lead to EEs, as we explain in the following section.

III. ROUTE TO SUPEREXTREME EVENTS

In this section, we show how the modification of the CO_2 laser modulation parameters gives rise to EEs, with the possibility of events with exceptionally large amplitudes when compared to the average amplitude of the laser intensity oscillations.

By varying the modulation parameters of the CO_2 laser, is well known that, when the modulation frequency is near the relaxation oscillation frequency, the laser has a number of phenomena and dynamical instabilities [44–51]. In particular, the laser exhibits the usual route to chaos via subharmonic (or period-doubling) bifurcations, as shown much earlier [42].

In Fig. 1 we show a phase diagram illustrating various instabilities occurring in the CO_2 laser, as a function of the modulation parameters. Briefly, the main instabilities to which we refer are as follows: (a) starting from the period-1 orbit, a sequence of subharmonic bifurcations occurs until the appearance of chaos, denoted by region I; (b) new periodic orbits are created through saddle-node bifurcations of limit cycles, denoted by the numbers 3, 4, 5, 6, and 7, which refer to the period of the orbits (these saddle-node bifurcations are sometimes called *primary saddle-node bifurcations* [47]); (c) each periodic orbit created develops a sequence of subharmonic bifurcations, leading to different chaotic regions in parameter space, which we denote by III, IV, V, VI, and VII; and (d) typically, each chaotic region ends when a crisis occurs [53]. In this work, we focus on the crisis denoted by the dashed line in Fig. 1, where there is a transition between the chaotic region I and the other chaotic regions. For the sake of clarity, we classify the chaotic regions in a hierarchical order. The chaotic region I is the lowest order, and we refer to the other chaotic regions as *higher-order chaotic regions* (or *chaotic bands*), where, for simplicity, we associate the "order" of the chaotic region with the period of the primary saddle-node bifurcation that gives rise to it.

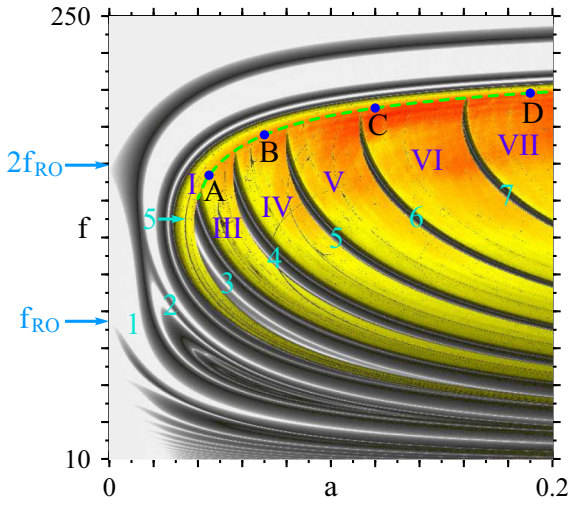

FIG. 1. Phase diagram of the CO_2 laser model as a function of modulation parameters. The diagram was computed through the Lyapunov exponents method [51]. Gray shades denote periodic solutions, and yellow-red shades denote chaotic solutions. The dashed line denotes the locus of a crisis between two chaotic attractors (see text for details). Arabic numbers indicate the period of some periodic regions, and roman numbers denote chaotic bands. Modulation parameters (a, f) are $A = (0.045, 163.725)$, $B = (0.070, 185.650)$, $C = (0.120, 200.170)$, and $D = (0.190, 208.250)$. The blue arrows in the vertical axis mark f_{RO} and $2f_{RO}$, i.e., modulation frequencies associated with the fundamental resonance and the main subharmonic resonance [48,52], respectively. Frequencies are in kHz.

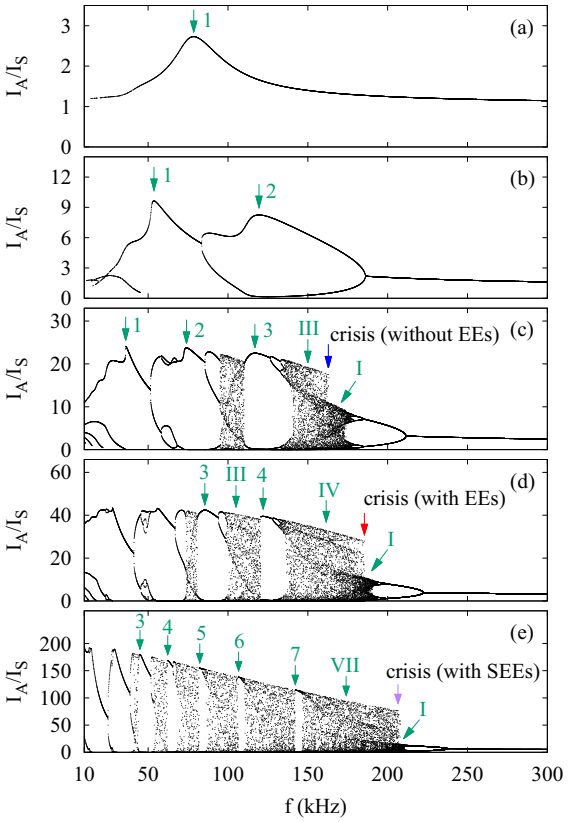

FIG. 2. Amplitude of the laser intensity pulses (I_A) as a function of modulation frequency. Arabic numbers denote the period of some periodic orbits, and roman numbers denote some different chaotic bands. The modulation amplitude is fixed in each diagram, and the values are (a) $a = 0.005$, (b) $a = 0.020$, (c) $a = 0.045$, (d) $a = 0.070$, and (e) $a = 0.190$. Other parameters are not changed. Green arrows denote resonant solutions, i.e., the largest intensity responses for a sequence of different periodic orbits. The blue arrow [in (c)] denotes a crisis without EEs, the red arrow [in (d)] denotes a crisis with EEs and the purple arrow [in (e)] denotes a crisis with SEEs.

It is important to mention that the chaotic regions to which we refer here are densely populated with periodic windows [51]. Each periodic window created by a saddle-node bifurcation develops a sequence of subharmonic bifurcations leading to the appearance of different chaotic regions. So, strictly speaking, the parameters where chaotic behaviors occur are not continuous, but they form a complicated fractal structure. For simplicity, we call the regions I, III, IV, etc., "chaotic regions" (or "chaotic bands"), without worrying about their internal structures. Another consequence of the periodic windows embedded in the chaotic regions is that the crisis line may not form a continuous segment. It was shown that a crisis line, for the case of another type of crisis, i.e., a boundary crisis, contains gaps and is divided into segments that form a fractal structure [54]. Again, for simplicity, we use the term "line" to denote the locus of the investigated crisis, without worrying about its fine structure.

Since we are interested in investigating EEs, i.e., rare light pulses emitted with large amplitude, it is worthwhile to keep in mind how large-amplitude events appear in the laser, when we vary the modulation parameters. Dynamically, the laser is a nonlinear damped oscillator with a parametric modulation, i.e., a nonlinear oscillator subject to a periodic perturbation. For low modulation amplitude, the laser response to a periodic perturbation is approximately linear. It is well known that, in a linear damped oscillator subject to a periodic perturbation, the largest oscillation amplitude occurs at the resonance frequency, i.e., when the perturbation frequency is equal to the natural oscillation frequency. Figure 2(a) illustrates this case approximately linearly, where the amplitude of the laser intensity oscillations is plotted against the modulation frequency for low modulation amplitude. In this case, we clearly observe the resonance when the modulation frequency coincides with the relaxation oscillation frequency.

When the modulation amplitude increases, nonlinear phenomena become important, as shown in Figs. 2(b)–2(e). Figure 2(b) illustrates the case in which the period-1 oscillation bifurcates to a period-2 oscillation. In this case, it is observed that each of the periodic orbits has a maximum amplitude response (shown by green arrows) for specific levels of modulation frequency. That is, each periodic solution has its own resonant frequency. The largest value of the laser amplitude response (global maximum) remains the period-1 oscillation. Notice that the resonance frequency of the period-1 solution has been shifted and is less than f_{RO} (i.e., it is redshifted).

For higher levels of modulation amplitude, chaotic oscillations occur and new periodic solutions are created through saddle-node bifurcation of limit cycles, as illustrated by Figs. 2(c)–2(e). Again, each periodic orbit has its own resonant

frequency (shown by green arrows). These created orbits follow a route of subharmonic bifurcations and give rise to the chaotic bands already mentioned. The interaction between different chaotic bands can lead to large variations in amplitude of the laser intensity oscillations. Notice that the largest oscillation amplitudes remain from the fundamental resonance, i.e., when $f \sim f_{\mathrm{RO}}$. However, for these modulation frequencies, the large-amplitude oscillations are very common, and the laser pulses do not display an EE statistics (with a long tail). The situation completely changes when considering modulation frequencies around the subharmonic resonance, i.e., when $f \gtrsim 2f_{\mathrm{RO}}$. In this case, the chaotic region I exhibits small-amplitude oscillations, and large intensity variations can occur when this chaotic region interacts with other chaotic bands (which display larger amplitudes). When moving from the chaotic region I to the other chaotic regions (by decreasing the modulation frequency), the small-amplitude chaotic attractor that exists in the region I undergoes a sudden expansion to a larger chaotic attractor. In the case we investigate here, this occurs when an unstable period-3 orbit (a saddle branch that is born through a saddle-node bifurcation) touches the chaotic solution that lies in the region I. This process, that is, the sudden size variation of the chaotic attractor due to the collision with an unstable periodic orbit, has been called by different names in the literature, such as *interior crisis* [53,55], *explosive bifurcation* [56], or *external crisis* [57]. To illustrate the usage of different nomenclature, in examples relating to a CO_2 laser, see, e.g., Refs. [33,58]. The locus of this crisis, in the frequency-amplitude space (a, f), is denoted by the dashed line in Fig. 1. The blue, red, and purple arrows in Figs. 2(c)–2(e) denote the occurrence of the crisis and illustrate the amplitude variations of the interaction between the chaotic region I and the chaotic regions III, IV, and VII, respectively. It is important to mention that the occurrence of a crisis does not necessarily imply the appearance of an EE, since the amplitudes of the oscillations should satisfy some previously arbitrated definition of an EE, as we discuss below.

When the modulation parameters are set for the laser operation in the chaotic regions III, IV, etc., sufficiently near the crisis line, abrupt amplitude variations can occur in the laser intensity oscillations. Figure 3(a) shows a typical time series of the laser intensity when the laser operates in region III, near the crisis (corresponding to point A in Fig. 1). As usual, to check quantitatively whether or not a given event meets the EE criterion (or rogue event criterion), we compare the intensity amplitude of the event with the average of the events plus a number n of standard deviations, σ, that we call the $n\sigma$ criterion (see, e.g., [59] or [23,29]). We denote as σ_I the standard deviation of the average intensity, $\langle I \rangle$, and σ_A denotes the standard deviation of the average peak amplitude, $\langle I_A \rangle$. Alternatively, it is possible to use an EE definition based on the calculation of the abnormality index, $\mathrm{AI} \equiv I_A / I_{A_{1/3}}$, where I_A is the amplitude of the intensity pulses, and $I_{A_{1/3}}$ is the "significant intensity," which is the average of the one-third highest amplitudes (as the "significant wave height" definition, in rogue wave studies). Usually, every amplitude with $\mathrm{AI} > 2$ is defined as an EE (or a rogue event) (see, e.g., [1,60] or [4,5]). The probability distribution function (PDF) of the laser intensity (where the statistics is performed for all intensity values, taken at each step h of integration) is shown in Fig. 3(b).

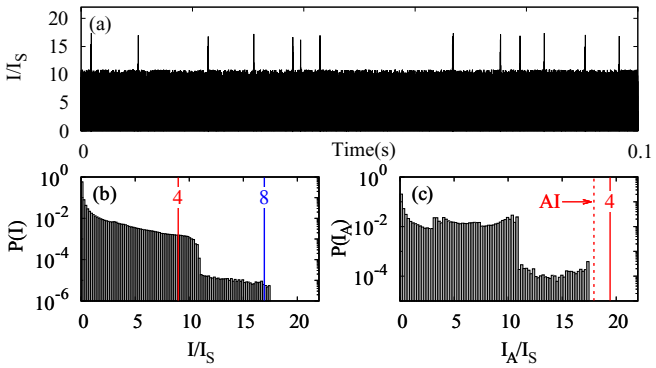

FIG. 3. Temporal behavior of the laser intensity (a) and the respective PDF (b). PDF of the pulse amplitude (c). Solid lines mark EE definitions, and numbers correspond to how many standard deviations exceed the average of the events. The dashed line marks another EE definition based on $\mathrm{AI} = 2$. Modulation parameters correspond to point A in Fig. 1 ($a = 0.045$, $f = 163.725$ kHz).

By applying the definition $I_{\mathrm{EE}} = \langle I \rangle + n\sigma_I$, intensity events exceeding I_{EE} are easily obtained for $n = 4$ or even 8. When we perform the statistics of amplitude of the intensity pulses and apply the definition $I_{A_{\mathrm{EE}}} = \langle I_A \rangle + n\sigma_A$, no amplitude satisfies the 4σ criterion. The same situation occurs by using the AI criterion, where no EEs are found for this distribution [see Fig. 3(c)]. As we can see, the definitions based on the 4σ and AI criterion are not coincident, but they do not differ significatively, for this distribution. Both definitions are arbitrary and each one can be used to define an EE.

By comparing the histograms of intensity and amplitude [Figs. 3(b) and 3(c)], we found different results from what was observed in investigations with an optically injected semiconductor laser [23], where there were no significant differences between the intensity and amplitude statistics. This may be explained due to the particularity of the pulses emitted by each laser system. In the case of the modulated CO_2 laser, in the regime that we investigate here, pulses typically occur in the form of pronounced spikes, that is, the laser operates for a longer time with low intensity and eventually triggers a high-intensity pulse, causing the intensities close to zero to be much more frequent, in comparison with other intensities. This is not the case of the semiconductor laser, leading to the different statistical properties.

In this work, from this point on, we will only consider statistics of amplitude to investigate the occurrence of EEs, using the $n\sigma$ criterion. Thus, the intensity oscillations shown in Fig. 3 do not exhibit EEs. However, for higher levels of modulation amplitude, near the crisis line, EEs begin to be observed. This fact occurs because, when the modulation amplitude increases, the amplitudes of the chaotic oscillations in the region I do not grow much, but the amplitudes of the chaotic oscillations in the regions III, IV, etc., increase significantly. Accordingly, EEs with increasing amplitudes are observed. Figure 4 shows the PDFs of the amplitude and the respective time series of the laser intensity for some representative modulation parameters. The laser intensity oscillations corresponding to points B, C, and D, shown in Fig. 1, exhibit EEs satisfying the 4σ, 8σ, and 12σ criterion, respectively. Indeed, if we keep

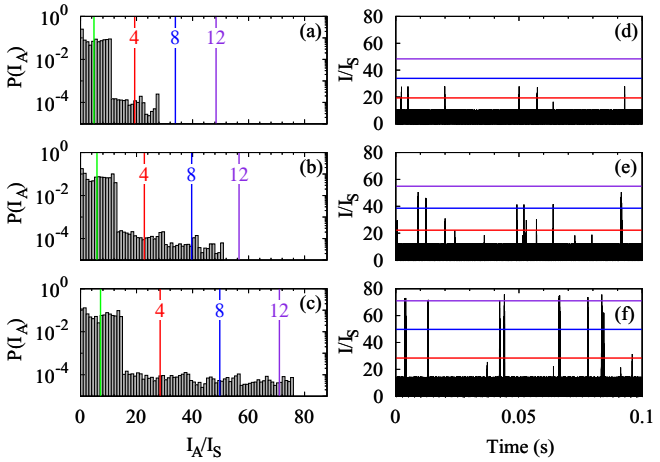

FIG. 4. Left column: PDFs of the pulse amplitude. The green lines denote the average amplitude ($\langle I_A \rangle$). Solid lines mark the EE definitions, and numbers correspond to how many standard deviations exceed $\langle I_A \rangle$. Modulation parameters (a, f) are (a) (0.070, 185.65 kHz), (b) (0.120, 200.17 kHz), and (c) (0.190, 208.25 kHz), corresponding to points B, C, and D in Fig. 1, respectively. Right column: The respective time series of the laser intensity.

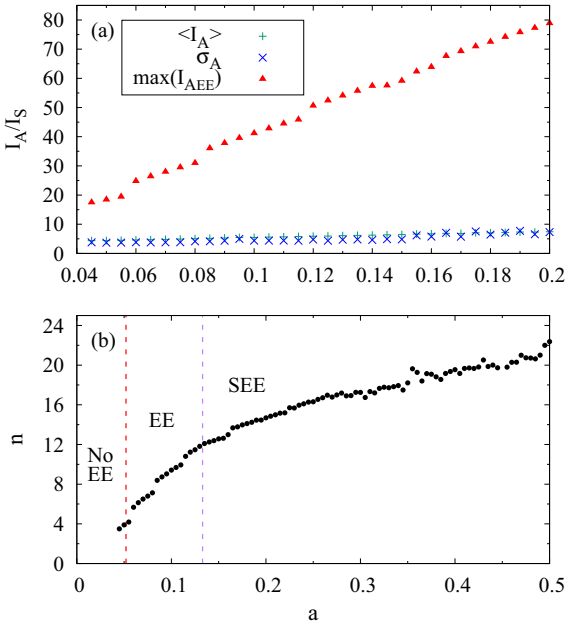

FIG. 5. (a) Maximum amplitude of EE, average amplitude ($\langle I_A \rangle$), and its standard deviation (σ_A) when the modulation parameters are varied slightly (50 Hz) below the crisis line. (b) Number of standard deviations (σ_A) exceeding the average amplitude of the laser pulses when the modulation parameters are varied over the crisis line. The red-dotted line and purple-dotted line mark the 4σ and 12σ criterion, respectively. "No EE," "EE," and "SEE" stand for "without extreme event," "extreme event," and "superextreme event," respectively, and they illustrate ranges of modulation amplitudes with increasing amplitudes for the observed rare events.

increasing the modulation amplitude, EEs with exceptionally large amplitudes are observed near the crisis line.

Figure 5 shows how the maximum amplitude of the EE varies as we increase the modulation amplitude, and, more importantly, how its deviation from the average amplitude increases significantly. In Fig. 5(a), the modulation parameters were varied near the crisis, in a representative case, with modulation frequencies 50 Hz below the crisis line. It is easy to observe that the amplitude of the EE increases considerably, whereas the average amplitude of the laser pulses, $\langle I_A \rangle$, and its standard deviation, σ_A, does not increase as much. This leads to EEs with increasing deviations in relation to the average amplitude (i.e., EEs exceeding a larger number of standard deviations relative to the average amplitude) when the modulation amplitude is increased. In Fig. 5(b), we compute the number n of standard deviations that exceeds the average amplitude of the laser pulses according to

$$n = \frac{\max\left(I_{A_{\mathrm{EE}}}\right) - \langle I_A \rangle}{\sigma_A}, \tag{6}$$

where $\max(I_{A_{\mathrm{EE}}})$ is the most EE found in an intensity time series after a large number of numerical integrations. It is important to realize that n depends on how far the modulation parameters are from the crisis, since both $\langle I_A \rangle$ and σ_A decrease when approaching the crisis (transversally) by increasing the modulation frequency. In Fig. 5(b) we estimate the limit case, that is, we compute n over the crisis line. For a fixed modulation amplitude, n starts to decrease when moving away from the crisis by decreasing the modulation frequency.

To understand how the system behaves near the critical transition (crisis), we analyze the dynamics of chaotic pulses in terms of the coefficient of variation, C_V, which is defined as the ratio of the standard deviation to the mean ($C_V = \sigma_A / \langle I_A \rangle$). The coefficient of variation is also called relative standard deviation (RSD), and it is sometimes expressed as a percentage. The main findings we obtained are illustrated in Fig. 6. Far away from the crisis, $\sigma_A > \langle I_A \rangle$, where we found typically $C_V \approx 2$. When approaching the crisis, both $\langle I_A \rangle$ and σ_A decrease, but at different rates, converging to $\sigma_A \approx \langle I_A \rangle$ close to the critical transition, and then $\sigma_A < \langle I_A \rangle$ when crossing the critical transition. Figure 6 gives us important insights about the behavior of the system

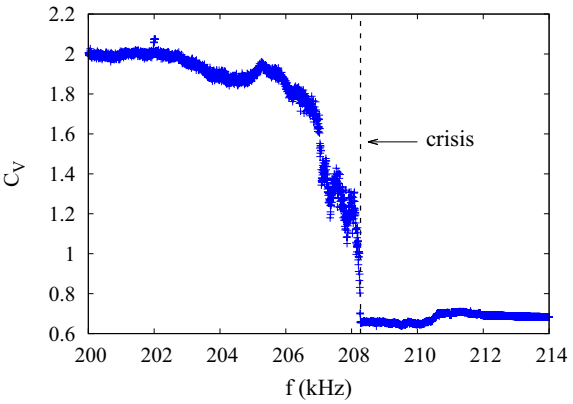

FIG. 6. The coefficient of variation ($C_V = \sigma_A / \langle I_A \rangle$) as a function of modulation frequency, when crossing the critical transition (crisis) for $a = 0.19$. The dashed line marks the crisis location ($f \approx$ 208.27 kHz).

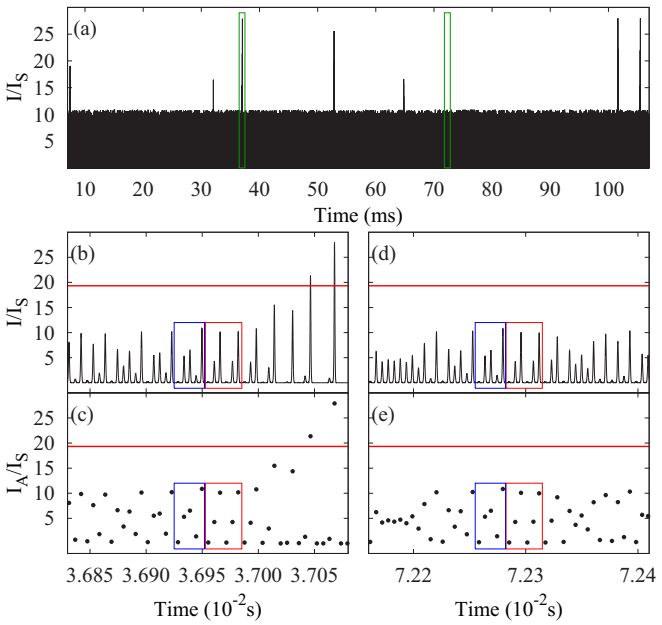

FIG. 7. (a) Temporal behavior of the laser intensity. The box on the left is magnified in (b) and the box on the right is magnified in (d). Parts (c) and (e) show only the amplitudes for the magnified boxes, respectively. The blue and red boxes are discussed in the text. The red lines denote the EE definition, according to the 4σ criterion. Modulation parameters correspond to point B in Fig. 1 ($a = 0.07, f = 185.65\,\text{kHz}$).

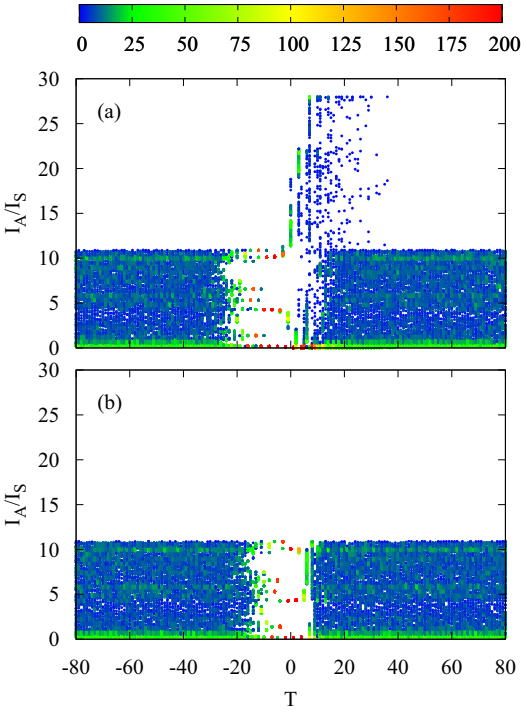

FIG. 8. Superposition of 200 time series (a) showing a regular pattern preceding an EE and (b) showing the same regular pattern without the emergence of an EE. Only the amplitudes of the laser pulses are plotted. T denotes the index of the successive local maxima of laser intensity. The color scale shows how many times each amplitude bin is visited (see text for details). Modulation parameters are as in Fig. 7.

close to the crisis bifurcation shown in Fig. 1 and its connection with the generation of large deviation events. We will come back to this point in Sec. V.

IV. PRECURSORS OF EXTREME AND SUPEREXTREME EVENTS

In this section, we consider the problem of prediction of EEs for the loss-modulated CO_2 laser. First, we investigate the existence of precursors of EEs, i.e., the existence of regular patterns that anticipate the occurrence of EEs. Second, and more importantly, we analyze the effectiveness of predicting an EE once a given precursor is identified.

By analyzing the time series of the laser intensity, when the modulation parameters are set to operate within the chaotic regions III, IV, etc., near the crisis line, we identified the existence of very regular patterns prior to the occurrence of EEs. Figure 7(a) shows a typical time series of the laser intensity, which corresponds to point B in Fig. 1. A magnification of this time series, in the vicinity of an EE, is shown in Figs. 7(b) and 7(c). A magnification of another part of the time series, far from the vicinity of an EE, is shown in Figs. 7(d) and 7(e). Regular patterns that exist embedded in the chaotic time series are shown highlighted by colored boxes. The red box shows two visitations to what resembles a period-3 orbit (with three different local maxima). We label this excursion in phase space (resembling a period-3 orbit) as a *pseudo-orbit of period three* (POP3). The blue box shows a visitation in phase space that resembles a period-5 orbit (with five different local maxima). We label this excursion in phase space as a *pseudo-orbit of period five* (POP5). Below, we show that these visitations in phase space occur recurrently in the chaotic time series, and we discuss their origin.

To show that these regular patterns appear recurrently in the chaotic time series of the laser intensity, where they may or may not anticipate the occurrence of EEs, we overlap many time series, starting from random initial conditions. Figures 8(a) and 8(b) show the superposition of 200 time series of the laser intensity, where only the amplitudes of the laser pulses are plotted. The overlays of the time series were performed as explained below. In Fig. 8(a), every time an EE is found, that is, when the intensity exceeds a certain threshold, we center the time series in this position and plot the 80 previous maxima and the 80 subsequent maxima. (To simplify the visualization, we take care to select pieces of time series in which only one EE is displayed in the considered time interval.) On the horizontal scale, instead of precisely indicating the occurrence time of the maxima, we simply use the occurrence index of the maxima, denoted by T. In Fig. 8(b), we identify numerically different POP3s that are not followed by the occurrence of an EE. The superposition of the time series was done centered on a local maximum of the POP3 and then by plotting the 80 previous maxima and the 80 subsequent maxima. To obtain information about the frequently visited regions of many different laser intensity trajectories in phase space, the vertical scale in Fig. 8 was divided into 60 bins, and a histogram for each T is shown in the color scale. In this way, we can clearly identify regular

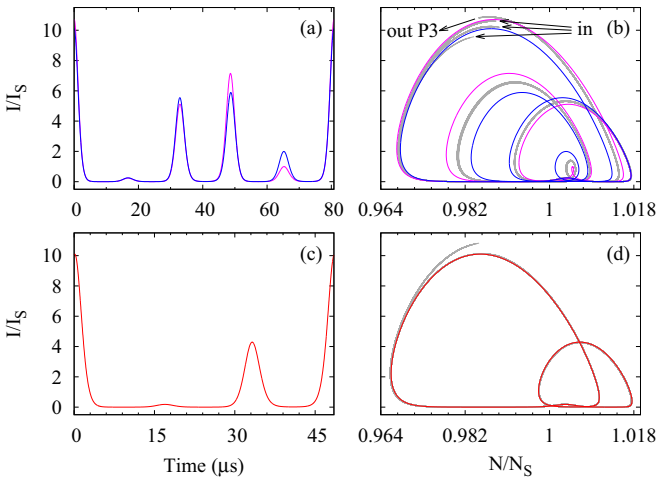

FIG. 9. (a) Time traces of two unstable period-5 orbits of laser intensity (magenta and blue lines) and (b) projection in phase space (I,N). (c) Time trace of an unstable period-3 orbit of laser intensity (red line) and (d) projection in phase space (I,N). In gray, in the panels (b) and (d), is shown the superposition of 50 visitations along POP5 and POP3, respectively. Modulation parameters are as in Fig. 7.

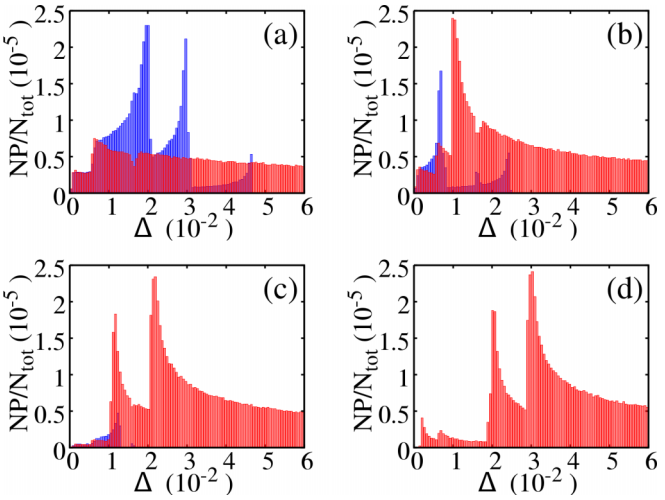

FIG. 10. In blue: number of precursors identified leading to the emergence of an EE. In red: number of precursors identified corresponding to false alarms, i.e., not leading to the emergence of an EE. The number of precursors (NP) identified in each case is normalized to the total number of local maxima ($N_{\rm tot} = 7.4 \times 10^8$) of each spanned time series. Δ is proportional to the precision in which a precursor is identified (see text for details). The modulation amplitude is fixed at $a = 0.07$. The modulation frequency is varied in each panel: (a) $f = 185.650\,$kHz (corresponding to point B in Fig. 1), (b) $f = 185.660\,$kHz, (c) $f = 185.665\,$kHz, and (d) $f = 185.669\,$kHz.

patterns formed by visitations containing POP5 followed by POP3. After this regular pattern, the emergence of an EE may or may not occur.

Below, we examine the origin of these regular patterns, formed by POP5 and POP3, which may occur with or without the emergence of an EE. As discussed in the previous section, with the variation of the modulation parameters, the laser shows a number of dynamic instabilities. Stable and unstable orbits are born through saddle-node bifurcations of limit cycles. When stable orbits undergo a subharmonic bifurcation, they do not disappear and continue to exist, but in an unstable form. Thus, there is a plethora of unstable periodic orbits embedded in the chaotic phases (in fact, an infinite number), making the dynamics in phase space rather complicated. Despite the complicated dynamics, with the usual sensitivity to initial conditions, the laser chaotic dynamic displays certain recurring regular patterns, such as the POP3 and POP5 discussed here. We can associate these regular patterns with the existence of unstable periodic orbits that are embedded in the chaotic phases. To elucidate this point, we compute some unstable periodic orbits for Eq. (1), using the software for numerical continuation, AUTO [61]. Figure 9(a) shows two unstable period-5 orbits. These orbits are born by a saddle-node bifurcation of a limit cycle, which forms a period-5 window (marked by an arrow in Fig. 1). At birth, one of the orbits is stable and one is unstable, but, for the modulation parameters that we investigate here, both orbits are unstable (since the stable orbit loses its stability in a subharmonic bifurcation). Figure 9(b) shows a projection of these two orbits in phase space (I,N). Together with these two unstable period-5 orbits, we plot the superposition of many POP5s (in gray), obtained by numerical integration of 50 different time series. We can observe that trajectories, coming from different regions in phase space, are trapped between the two unstable period-5 orbits, forming the POP5. After the excursion along the POP5, the trajectories are mapped to the vicinity of an unstable period-3 orbit [see Figs. 9(c) and 9(d)]. This unstable period-3 orbit is born (already in an unstable form) by a saddle-node bifurcation of limit cycle, which gives rise to a period-3 window (marked in Fig. 1). (Another period-3 orbit, which is born stable and loses its stability in a subharmonic bifurcation, is located in a more distant position in phase space and is not shown here.) Figure 9(d) shows a projection in phase space (I,N) of the unstable period-3 orbit (red curve) together with the superposition of 50 trajectories of POP3s (gray curves). The POP3 trajectories perform very close excursions to the vicinity of the unstable period-3 orbit. After one or more excursions in the vicinity of the unstable period-3 orbit, two possibilities follows: either the trajectory is mapped to the large-amplitude portion of the chaotic attractor, with the occurrence of an EE, or the trajectory is mapped to the small-amplitude portion of the chaotic attractor, without the occurrence of an EE. Due to the fact that, whenever there is an EE, it is preceded by POP3, we can use the POP3 as a *precursor* for the emergence of an EE. However, the occurrence of a precursor is not always associated with the emergence of an EE. This situation is analyzed below.

Since not all precursors found in the time series of the laser intensity lead to the emergence of an EE, an important question is as follows: what is the probability of the emergence of an EE once a precursor is identified in the time series? To answer this question, we perform some numerical simulations, which are summarized in Fig. 10. Using the known unstable period-3 orbit as a precursor (computed numerically with AUTO, within a given numerical accuracy), we compare all the amplitudes of the laser pulses in a very long time series with the amplitudes of the unstable period-3 orbit, in accordance with the

expression

$$\Delta(t) = \frac{1}{6I_S} \sum_{i=1}^{6} \min_{j=1,2,3} \left| I_{A_{T-i}} - I_j^* \right|, \tag{7}$$

where the set I_j^* ($j = 1,2,3$) are the local maxima (amplitudes) of the unstable period-3 orbit of the laser intensity, and the number 6 is related to the minimum length (two excursions in the vicinity of the unstable period-3 orbit) of POP3. Thus, Δ is related to the accuracy with which we can determine the precursor (POP3).

In Fig. 10, we plot in blue (red) a histogram of the values of Δ leading (not leading) to the emergence of an EE. This figure is directly related to the number of precursors found in the time series as a function of the defined accuracy. We can see that the visitations along the POP3 are rare. Our results show that the probability of predicting an EE in the deterministic time series depends on the distance between the trajectory in phase space and the unstable period-3 orbit used as a precursor. In other words, this probability depends on the accuracy with which the precursor is identified. For example, in Fig. 10(a) (which corresponds to point B in Fig. 1), for $\Delta < 0.005$, the number of precursors identified that lead to an EE is about the same as the number that do not lead to an EE. In this case, the probability of correctly predicting an EE is 50%. However, for larger values of Δ, this probability varies widely, as we can see in the histogram. Depending on the value of Δ, we may have more precursors leading to an EE than not leading to one, or vice versa. From a certain value of Δ, we move too far from the POP3, and precursors identified with this accuracy do not lead to the emergence of an EE. To evaluate how sensitive these computed probabilities are with respect to parameter variations, we repeat the same calculations for other modulation frequencies when moving in a closely transverse direction of the crisis. The results are shown in Figs. 10(b)–10(d). As we approach the crisis, the EEs are increasingly rare [Figs. 10(b) and 10(c)]. When we cross the crisis [Fig. 10(d)], the laser operates within the chaotic region I (where only small-amplitude chaotic dynamics occurs), and no EEs are observed in the deterministic case that we investigate here.

V. DISCUSSION

The main mechanism of EE formation that we report here is related to the interaction between a chaotic region arising from the instability of the fundamental periodic solution (the period-1 solution) with chaotic bands arising from instabilities of periodic orbits of period 3, 4, 5, 6, 7, etc., created by saddle-node bifurcations of limit cycles. At the beginning of the interaction between the chaotic region I and the chaotic region III, through a crisis, the amplitudes of the chaotic attractors do not differ significantly, and therefore there is no EE statistics. For a certain level of modulation amplitude, the amplitudes of the chaotic attractors become more different, and EE statistics start to be observed. Since we are looking at transitions between the chaotic region I to other higher-order chaotic regions, i.e., I $\rightarrow$ III, I $\rightarrow$ IV, I $\rightarrow$ V, etc., the higher the modulation amplitude is, the larger is the amplitude of the EE when compared to the average amplitude. Previous EE statistics in a loss-modulated CO_2 laser was reported in Ref. [33], with EEs arising from interaction between neighboring chaotic bands, such as III $\rightarrow$ IV, IV $\rightarrow$ V, V $\rightarrow$ VI, etc. The case we show here differs from this previous investigation since we are considering interactions between a low-order chaotic band with other higher-order chaotic bands, as already explained.

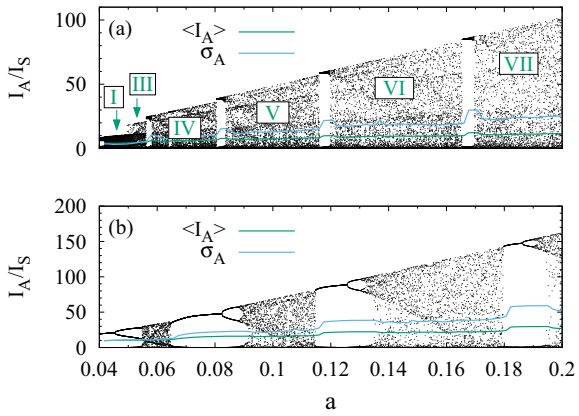

FIG. 11. Bifurcation diagrams illustrating some differences in amplitudes for successive branches of intensity solutions. (a) Strongly resonant case ($f \approx f_{RO}$), where $f = 85$ kHz. (b) Weakly resonant case ($f \approx 2f_{RO}$), where $f = 170$ kHz. Roman numbers denote different chaotic bands.

To understand better the mechanism of the emergence of large-deviation EEs, which we describe here, it is illustrative to have an overview of how amplitudes grow when we increase the modulation amplitude, at different modulation frequencies. Figure 11(a) shows the amplitude variations of different chaotic bands (denoted by roman numerals) for $f \approx 2f_{\mathrm{RO}}$. The chaotic band I corresponds to entire chaotic region above the crisis line in the modulation parameter space, whereas the other higher-order chaotic bands are located below the crisis line. When the modulation amplitude increases, amplitudes of chaotic band I grow very little. Then we refer to the intensity oscillations of chaotic band I as *weakly resonant* solutions, i.e., intensity oscillations whose amplitudes do not grow much when the modulation amplitude increases [to check amplitude variations of the chaotic band I for higher levels of modulation amplitude, see Figs. 2(c)–2(e)]. On the other hand, amplitudes of higher-order chaotic bands grow significantly as the modulation amplitude increases. Then we refer to the intensity oscillations of chaotic bands III, IV, etc., as *strongly resonant* solutions, i.e., intensity oscillations whose amplitude increases significantly as the modulation amplitude increases. As we move toward the resonance frequency, the amplitudes of the intensity oscillations become even larger, as can be seen in Fig. 11(b), for $f \approx f_{\mathrm{RO}}$. But in this strongly resonant regime, when the modulation amplitude increases, the average and dispersion of the amplitudes increase considerably [see the green and blue lines in Fig. 11(b)]. Thus, for high modulation amplitude and $f \sim f_{\mathrm{RO}}$, the laser pulses exhibit very large amplitudes, but also very large variability. For example, for $a = 0.2$ and $f = 85$ kHz, it is found that $\langle I_A \rangle \approx 26$ and

$\sigma_A \approx 51$. When moving toward the crisis, the average and dispersion of amplitudes decrease (e.g., $\langle I_A \rangle \approx 12$ and $\sigma_A \approx 25$ for $a = 0.2$ and $f = 170$ kHz) until a transition is observed through the crisis in the same way as is shown in Fig. 6. In other words, when moving from the resonance frequency toward the crisis (by increasing the modulation frequency), at some stage, the pulses start to get more and more "clustered" around the average value, since the dispersion of amplitudes decreases faster than the average. When approaching very close to the crisis, the laser oscillations "feel" strongly the interaction with the small-amplitude and small-dispersion chaotic attractor that is found after the crisis. Before crossing the crisis, although the amplitudes have a small average and small dispersion, eventually very intense pulses can be emitted since the chaotic attractor that lies before the crisis has a very large amplitude.

Thus, the mechanism described in this article explains the emergence of rare laser pulses with exceptionally large amplitudes, including events with amplitudes that deviate significantly from the 4σ criterion. In the same way that we can arbitrarily define EEs as those satisfying the 4σ criterion (or 8σ, to be more restrictive), we could arbitrarily define SEEs as those satisfying the 10σ criterion (or 12σ, to be more restrictive), as we suggested in Figs. 2(e) and 5(b). More important than saying how many "σ" is the SEE definition, since this definition is also arbitrary, is to understand how EE deviation increases relative to the average amplitude when system parameters are changed, as we did in Fig. 5(b). We found EEs with deviations in the range from 4σ to 20σ, while EEs are usually reported with deviations in the range from 4σ to 8σ. This is a significant difference, not only because *quantitatively*, of course, a 10σ event could have a much higher potential for impact than a 4σ event, but mainly because the events with increasing deviations are related to different order solutions, i.e., they are *qualitatively* different, as we showed in this article. This discovery leads us to suggest that "superextreme and rare events" exist in low-dimensional chaotic systems, in analogy with Ref. [41], where "super rogue waves" were discovered in water waves, when investigating EEs in high-dimensional systems. It is remarkable that in Ref. [41], the super rogue waves are related to higher-order rational solutions of the nonlinear Schrödinger equation, whereas in the case presented here the SEEs are related to higher-order chaotic regions, which in turn originate from higher-order primary saddle-node bifurcation of limit cycles. The results presented here suggest that there may be a close connection between the higher-order rogue waves solutions and the primary saddle-node bifurcations observed here.

As shown in Sec. III, the occurrence of a crisis does not guarantee the observation of EE statistics, i.e., it is not a sufficient condition to observe an EE. Obviously, it is necessary to *satisfy* a criterion that defines an event to be an EE (or rogue event). But what else, beyond crisis, is behind the formation of an EE? Certainly, resonance is a key element to the formation of an EE in low-dimensional nonlinear systems, as we investigate here. In fact, nonlinear resonant processes, leading to the formation and interaction of different branches of solutions (arising from fundamental, harmonic, and subharmonic resonances), can lead to a significant spread of amplitudes of the events, being a key element to display EE

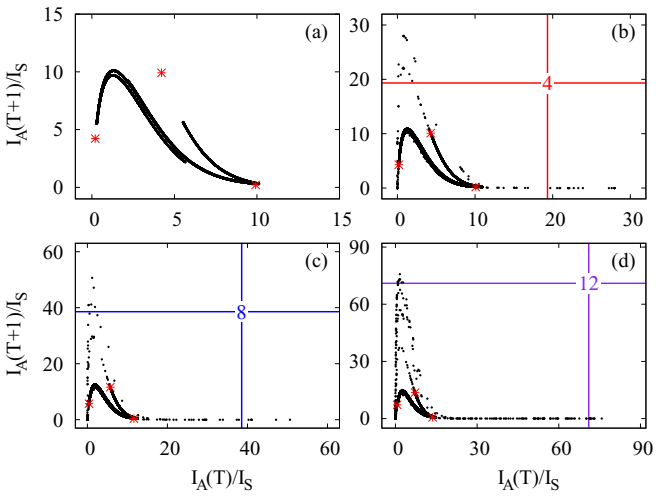

FIG. 12. Return maps of the laser pulse amplitude. Black points correspond to the chaotic attractor and red points to unstable period-3 orbit. The lines and numbers are as in Fig. 4. Modulation parameters (a, f) are (a) (0.07, 189.000 kHz), (b) (0.07,185.650 kHz), (c) (0.12,200.170 kHz), and (d) (0.19,208.250 kHz). Each return map was done with 20 000 pulse amplitudes.

statistics. From a more fundamental point of view, we could think of *synchronization or constructive interferences* as key elements for extreme wave generation in high-dimensional systems. In a low-dimensional nonlinear system, however, *nonlinear resonances*, leading to interaction between strong (higher-order) and weak (lower-order) resonant solutions, play a very important role in EE generation.

Regarding our study on predicting EEs, the regular pattern identified in Sec. IV, which is embedded in the chaotic time series and can be used to anticipate the EE, is not restricted only to the investigated parameter (point B in Fig. 1). The same regular pattern typically occurs in time series taken near the crisis, over the entire extension of the crisis line. This regular pattern is a feature of the transition from region I to the other chaotic bands. In Fig. 12 we show some representative return maps for modulation parameters near the crisis line. Figure 12(a) shows the chaotic attractor within the region I and an unstable period-3 orbit, which coexist with the chaotic attractor. When we approach the crisis line, eventually the unstable period-3 orbit touches the chaotic attractor, leading to the crisis. After the crisis, a sudden expansion of the chaotic attractor is observed. Figure 12(b) shows a return map after the crisis, corresponding to point B in Fig. 1. The same qualitative picture, found in the transition to point B, is observed for other modulation parameters near the crisis line [for example, points C and D, as shown in Figs. 12(c) and 12(d)]. The most pronounced difference, when investigating other modulation parameters along the crisis line, is the size of the amplitude variations of the EE, as already discussed in Sec. III. Since the crisis occurs via collision with an unstable period-3 orbit, this explains the periodicity of the precursor that we have identified preceding the EE, i.e., the POP3. When other periodic orbits are involved in the crisis formation, for example period 4, 5, etc., other periodicities of precursors can be

found, respectively, anticipating the EE. An investigation in this direction is left for future work.

Regular patterns preceding the occurrence of an EE have been observed previously in low-dimensional chaotic systems, such as semiconductor lasers [32] and solid-state lasers [35], and also in high-dimensional turbulent systems [40]. However, here we show that the same regular pattern, which appears preceding the EE, can also appear without the emergence of an EE. In this case, the precursors found in the time series, which are not followed by the occurrence of an EE, can be considered as *false alarms*.

Previous investigations of EEs have found a narrow region in phase space that a trajectory has to visit to trigger an EE. The authors have referred to this region as the "narrow rogue wave door" [32] or "channel-like structure" [34]. In our work, we have estimated the width of these narrow regions since the width of the blue histograms (shown in Fig. 10) is closely related to the width of the phase space that the trajectories have to visit to trigger an EE. We have also illustrated how the width of this narrow channel decreases when we approach the crisis, causing the EE to occur less frequently, until it cannot be observed anymore (after the crisis). Notice that this latter result is in agreement with previous theoretical and experimental investigations of the number of EEs when changing parameters in a transverse direction to the crisis [33,35].

Despite the relative simplicity of the system investigated (as can be observed through inspection of the return maps in Fig. 12, typical of low-dimensional chaos), which is a noise-free system and which we know the orbit used as a precursor (within a good precision), we already found a complicated dependence on the probability to predict an EE as a function of the accuracy used to identify the precursor. It is natural to expect additional complications in more complex systems, which motivate us to carry our further investigations.

Since nonlinear resonances and instabilities are very common phenomena in nonlinear systems, we believe that our findings can have a big impact beyond the selected example, including other parametric oscillators, external forced oscillators, or even autonomous systems. The results shown here could be directly applied to certain systems involving the Toda potential, since the laser model investigated here was shown to be fully equivalent to the Toda oscillator in the past [62]. From an experimental point of view, we expect that the main results shown in this work could be observed in real-world systems, such as modulated lasers or other physical systems. An interesting investigation would be to search for superextreme and rare events in some controlled experiment or to verify if the same regular patterns that occur preceding the EE can also occur without the emergence of the EE, and to try to quantify the probability of occurrence of EEs and false alarms, as we did here. We hope to work in this direction in the near future.

VI. CONCLUSION

We investigated numerically the emergence of extreme and rare events, i.e., giant and rare light pulses, in a simple deterministic model of a loss-modulated CO_2 laser. We identified a crisis line in the modulation parameter space where a transition between a small-amplitude chaotic attractor and other successive chaotic attractors of larger amplitudes occurs. We showed that, when the modulation amplitude is increased, remaining close to the crisis, the average and dispersion of the laser pulse amplitudes change very little while the amplitudes of the extreme pulses grow enormously, giving rise to events with much larger deviations than usually reported. Normally extreme (or rogue) events are found with amplitudes that deviate slightly more than four or eight standard deviations (over average amplitude), and here we found EEs with deviations in the range from 4 to 20 standard deviations, i.e., we showed the possibility of the formation of EEs that exceeds significantly the 4σ (8σ) criterion, with a significant probability of occurrence, which we called "superextreme events."

We explained the mechanism of the formation of superextreme events through the interaction between weakly resonant chaotic attractors (whose amplitudes do not grow much when the modulation amplitude increases) and strongly resonant chaotic attractors (whose amplitudes grow significantly when the modulation amplitude increases). We showed that the EEs with increasing deviations are *qualitatively* different, since they are related with higher-order chaotic bands, i.e., chaotic bands that originate from different primary saddle-node bifurcations. Thus the superextreme events could be thought of as originating from different solution classes.

We investigated the transition from a high-order chaotic attractor (order VI) to a low-order, weakly resonant chaotic attractor (order I), through a crisis bifurcation, in terms of the coefficient of variation (C_V), that is, the ratio between the standard deviation normalized to its average value. We showed that far away from the crisis (toward strongly resonant solutions), $C_V > 1$, and when approaching the crisis (toward weakly resonant solutions) the coefficient of variation starts to decrease, converging to $C_V \approx 1$, very close to the crisis, and $C_V < 1$ when crossing the crisis. The investigated crisis can be thought of as a transition between a "less clustered state" (amplitudes with large deviations in relation to the average) to a "more clustered state" (amplitudes deviating very little in relation to the average). Close to the border of this transition, EEs with extremely large deviations are expected to occur, depending on the order of the strongly resonant solution.

We identified regular patterns in the time series of the laser intensity, which may act as precursors and anticipate the occurrence of an EE, and we associated these precursors with certain unstable periodic orbits that are embedded in the chaotic attractor, which rules the laser dynamics. We showed that these precursors may appear recurrently in the time series of the laser intensity with or without the emergence of an EE. Thus, we estimated the probability of predicting EEs or having false alarms once a precursor is identified. We showed that the probability of predicting the EE depends on the accuracy with which we determine the precursor in the chaotic time series.

Further work is required to clarify some additional points. It would be relevant to make a comparison with more realistic CO_2 laser models, such as those involving a fully molecular description [63–65], where new ingredients and additional features could be involved, possibly leading to some extra saturation mechanism. Also, it would be important to analyze the impact of noise, always present in real-world systems, in the formation and prediction of large-deviation EEs. From a more general point of view, a more challenging problem would be to perform an analysis similar to the one we performed

here on systems with additional degrees of freedom, such as that exhibiting return maps more complicated, including hyperchaotic dynamics and robust chaos. We hope to present results in this direction in the future.

ACKNOWLEDGMENTS

C.B. thanks CNPq (Conselho Nacional de Desenvolvimento Científico), Brazil, and A.E. thanks FAPERGS, Brazil, for financial support.

[1] C. Kharif, E. Pelinovsky, and A. Slunyaev, *Rogue Waves in the Ocean* (Springer, Heidelberg, 2009).
[2] D. R. Solli, C. Ropers, P. Koonath, and B. Jalali, Nature (London) **450**, 1054 (2007).
[3] M. Onorato, S. Residori, U. Bortolozzo, A. Montina, and F. T. Arecchi, Phys. Rep. **528**, 47 (2013).
[4] J. M. Dudley, F. Dias, M. Erkintalo, and G. Genty, Nat. Photon. **8**, 755 (2014).
[5] C. Liu, R. E. C. van der Wel, N. Rotenberg, L. Kuipers, T. F. Krauss, A. Di Falco, and A. Fratalocchi, Nat. Phys. **11**, 358 (2015).
[6] N. Akhmediev *et al.*, J. Opt. **18**, 063001 (2016).
[7] *Extreme Events and Natural Hazards: The Complexity Perspective*, edited by A. S. Sharma, A. Bunde, V. P. Dimri, and D. N. Baker (American Geophysical Union, Washington, D.C., 2013).
[8] *Extreme Events: Observations, Modeling, and Economics*, edited by M. Chavez, M. Ghil, and J. Urrutia-Fucugauchi (Wiley, Hoboken, 2016).
[9] *Extreme Events in Finance: A Handbook of Extreme Value Theory and Its Applications*, edited by F. Longin (Wiley, Hoboken, 2017).
[10] R. Höhmann, U. Kuhl, H.-J. Stöckmann, L. Kaplan, and E. J. Heller, Phys. Rev. Lett. **104**, 093901 (2010).
[11] F. T. Arecchi, U. Bortolozzo, A. Montina, and S. Residori, Phys. Rev. Lett. **106**, 153901 (2011).
[12] J. J. Metzger, R. Fleischmann, and T. Geisel, Phys. Rev. Lett. **112**, 203903 (2014).
[13] A. Mathis, L. Froehly, S. Toenger, F. Dias, G. Genty, and J. M. Dudley, Sci. Rep. **5**, 12822 (2015).
[14] A. I. Dyachenko, D. I. Kachulin, and V. E. Zakharov, Stud. Appl. Math. **137**, 189 (2016).
[15] M. Mattheakis, I. J. Pitsios, G. P. Tsironis, and S. Tzortzakis, Chaos Solitons Fractals **84**, 73 (2016).
[16] S. Birkholz, C. Brée, I. Veselić, A. Demircan, and G. Steinmeyer, Sci. Rep. **6**, 35207 (2016).
[17] C. Kharif and E. Pelinovsky, Eur. J. Mech. B **22**, 603 (2003).
[18] A. I. Dyachenko and V. E. Zakharov, JETP Lett. **81**, 255 (2005).
[19] P. K. Shukla, I. Kourakis, B. Eliasson, M. Marklund, and L. Stenflo, Phys. Rev. Lett. **97**, 094501 (2006).
[20] F. Baronio, M. Conforti, A. Degasperis, S. Lombardo, M. Onorato, and S. Wabnitz, Phys. Rev. Lett. **113**, 034101 (2014).
[21] B. Kibler, A. Chabchoub, A. Gelash, N. Akhmediev, and V. E. Zakharov, Phys. Rev. X **5**, 041026 (2015).
[22] F. Fedele, J. Brennan, S. P. de León, J. Dudley, and F. Dias, Sci. Rep. **6**, 27715 (2016).
[23] C. Bonatto, M. Feyereisen, S. Barland, M. Giudici, C. Masoller, J. R. Rios Leite, and J. R. Tredicce, Phys. Rev. Lett. **107**, 053901 (2011).
[24] A. N. Pisarchik, R. Jaimes-Reátegui, R. Sevilla-Escoboza, G. Huerta-Cuellar, and M. Taki, Phys. Rev. Lett. **107**, 274101 (2011).
[25] S. Toenger, T. Godin, C. Billet, F. Dias, M. Erkintalo, G. Genty, and J. M. Dudley, Sci. Rep. **5**, 10380 (2015).
[26] P. Walczak, S. Randoux, and P. Suret, Phys. Rev. Lett. **114**, 143903 (2015).
[27] F. Selmi, S. Coulibaly, Z. Loghmari, I. Sagnes, G. Beaudoin, M. G. Clerc, and S. Barbay, Phys. Rev. Lett. **116**, 013901 (2016).
[28] A. Abrashkin and A. Soloviev, Phys. Rev. Lett. **110**, 014501 (2013).
[29] C. J. Gibson, A. M. Yao, and G.-L. Oppo, Phys. Rev. Lett. **116**, 043903 (2016).
[30] V. Odent, M. Taki, and E. Louvergneaux, Nat. Hazards Earth Syst. Sci. **10**, 2727 (2010).
[31] A. Karsaklian Dal Bosco, D. Wolfersberger, and M. Sciamanna, Opt. Lett. **38**, 703 (2013).
[32] J. Zamora-Munt, B. Garbin, S. Barland, M. Giudici, J. R. Rios Leite, C. Masoller, and J. R. Tredicce, Phys. Rev. A **87**, 035802 (2013).
[33] C. Metayer, A. Serres, E. J. Rosero, W. A. S. Barbosa, F. M. de Aguiar, J. R. Rios Leite, and J. R. Tredicce, Opt. Express **22**, 19850 (2014).
[34] R. Karnatak, G. Ansmann, U. Feudel, and K. Lehnertz, Phys. Rev. E **90**, 022917 (2014).
[35] N. M. Granese, A. Lacapmesure, M. B. Agüero, M. G. Kovalsky, A. A. Hnilo, and J. R. Tredicce, Opt. Lett. **41**, 3010 (2016).
[36] G. Nicolis and C. Nicolis, *Foundations of Complex Systems*, 2nd ed. (World Scientific, Singapore, 2012).
[37] S. Albeverio, V. Jentsch, and H. Kantz, *Extreme Events in Nature and Society*, The Frontiers Collection (Springer, Berlin, 2006).
[38] V. Keilis-Borok, A. Soloviev, and A. Gabrielov, in *Extreme Events: Observations, Modeling, and Economics* (Ref. [8]).
[39] D. Sornette, *Critical Phenomena in Natural Sciences*, edited by H. Haken (Springer, Berlin, 2006).
[40] S. Birkholz, C. Brée, A. Demircan, and G. Steinmeyer, Phys. Rev. Lett. **114**, 213901 (2015).
[41] A. Chabchoub, N. Hoffmann, M. Onorato, and N. Akhmediev, Phys. Rev. X **2**, 011015 (2012).
[42] F. T. Arecchi, R. Meucci, G. Puccioni, and J. R. Tredicce, Phys. Rev. Lett. **49**, 1217 (1982).
[43] V. N. Chizhevsky, Phys. Rev. E **64**, 036223 (2001).
[44] L. M. Narducci and N. B. Abraham, *Laser Physics and Laser Instabilities* (World Scientific, Singapore, 1988).
[45] H. G. Solari, E. Eschenazi, R. Gilmore, and J. R. Tredicce, Opt. Commun. **64**, 49 (1987).
[46] D. Dangoisse, P. Glorieux, and D. Hennequin, Phys. Rev. A **36**, 4775 (1987).
[47] I. B. Schwartz, Phys. Lett. A **126**, 411 (1988).
[48] T. Kurz and W. Lauterborn, Phys. Rev. A **37**, 1029 (1988).
[49] I. B. Schwartz and T. Erneux, SIAM J. Appl. Math. **54**, 1083 (1994).

[50] T. W. Carr, L. Billings, I. B. Schwartz, and I. Triandaf, Physica D **147**, 59 (2000).
[51] C. Bonatto, J. C. Garreau, and J. A. C. Gallas, Phys. Rev. Lett. **95**, 143905 (2005).
[52] J. M. T. Thompson and H. B. Stewart, *Nonlinear Dynamics and Chaos* (Wiley, Chichester, 2002).
[53] C. Grebogi, E. Ott, and J. A. Yorke, Physica D **7**, 181 (1983).
[54] H. M. Osinga, Phys. Rev. E **74**, 035201(R) (2006).
[55] K. T. Alligood, T. D. Sauer, and J. A. Yorke, *Chaos: An Introduction to Dynamical Systems* (Springer, New York, 1996).
[56] J. M. T. Thompson, H. B. Stewart, and Y. Ueda, Phys. Rev. E **49**, 1019 (1994).
[57] R. Gilmore, Rev. Mod. Phys. **70**, 1455 (1998).
[58] R. Meucci, E. Allaria, F. Salvadori, and F. T. Arecchi, Phys. Rev. Lett. **95**, 184101 (2005).
[59] K. Dysthe, H. E. Krogstad, and P. Müller, Annu. Rev. Fluid Mech. **40**, 287 (2008).
[60] H. U. Sverdrup and W. H. Munk, U. S. Navy Hydrographic Office, Pub. No. 601 (1947).
[61] E. J. Doedel, B. E. Oldeman, A. R. Champneys, F. Dercole, T. F. Fairgrieve, Y. Kuznetsov, R. C. Paffenroth, B. Sandstede, X. J. Wang, and C. H. Zhang, AUTO-07p, Version 0.7: *Continuation and Bifurcation Software for Ordinary Differential Equations* (Concordia University, Montréal, Canada, 2010).
[62] G.-L. Oppo and A. Politi, Z. Phys. B **59**, 111 (1985).
[63] T. Erneux and P. Glorieux, *Laser Dynamics* (Cambridge University Press, Cambridge, 2010).
[64] A. Varone, A. Politi, and M. Ciofini, Phys. Rev. A **52**, 3176 (1995).
[65] E. J. Doedel and C. L. Pando L., Phys. Rev. E **89**, 052904 (2014).